IEEE JOURNAL ON
SELECTED AREAS IN COMMUNICATIONS

Reliable and Efficient Sub-Nyquist Wideband Spectrum Sensing in Cooperative Cognitive Radio Networks

Yuan Ma, *Student Member, IEEE,* Yue Gao, *Senior Member, IEEE,* Ying-Chang Liang, *Fellow, IEEE,* and Shuguang Cui, *Fellow, IEEE*

***Abstract*— The rising popularity of wireless services resulting in spectrum shortage has motivated dynamic spectrum sharing to facilitate efficient usage of the underutilized spectrum. Wideband spectrum sensing is a critical functionality to enable dynamic spectrum access by enhancing the opportunities of exploring spectral holes, but entails a major implementation challenge in compact commodity radios that only have limited energy and computation capabilities. In contrast to traditional sub-Nyquist approaches where a wideband signal or its power spectrum is first reconstructed from compressed samples, this paper proposes a sub-Nyquist wideband spectrum sensing scheme that locates occupied channels blindly by recovering the signal support, based on the jointly sparse nature of multiband signals. Exploiting the common signal support shared among multiple secondary users (SUs), an efficient cooperative spectrum sensing scheme is developed, in which the energy consumption on wideband signal acquisition, processing, and transmission is reduced with detection performance guarantee. Based on subspace decomposition, the low-dimensional measurement matrix, computed at each SU from local sub-Nyquist samples, is deployed to reduce the transmission and computation overhead while improving noise robustness. The theoretical analysis of the proposed sub-Nyquist wideband sensing algorithm is derived and verified by numerical analysis and further tested on real-world TV white space signals. It shows that the proposed scheme can achieve good detection performance as well as reduce computation and implementation complexity, in comparison with conventional cooperative wideband spectrum sensing schemes.**

***Index Terms*— Wideband spectrum sensing, cooperative spectrum sensing, sub-Nyquist sampling, multicoset sampling, joint sparse recovery.**

I. Introduction

With the explosive proliferation of wireless devices and rapid growth of wireless services, spectrum scarcity has become a major bottleneck for wireless industry. The threat of spectrum shortage has encouraged the governments to take critical steps towards releasing multiple bands for dynamic spectrum sharing, motivated by the fact that the actual spectrum is underutilized in practice [2]–[4]. For instance, Fig. 1, collected by the RFeye node [5] located at Queen Mary University of London (QMUL) in London, United Kingdom, shows that a large portion of the spectrum remains unused. In particular, TV white space (TVWS) is one of the most promising section for dynamic spectrum sharing, which is composed of the channels that are not used by digital terrestrial televisions (DTT) or programme making and special events (PMSE) users, and those freed up by the switch-over from analogue to digital TV broadcasting [3], [6]. The UK communications regulator, Ofcom of Communications (Ofcom), has announced the licence exempt regulations for TVWS in December 2015 [7]. Compact and low-power white space devices for rural broadband/WiFi-like accesses and Machine-to-Machine (M2M) communications could therefore operate on these vacant channels without causing interferences to the primary transmissions [8], [9].

To enable dynamic spectrum access over TVWS, one needs fast and accurate detection of the surrounding spectrum that does not cause interferences to primary transmissions. One major current approach to discover available TVWS channels is using a Geo-location database [6]. However, this approach requires an initial wired or wireless link available at the master white space device in order to report its location to the central database [3]. Moreover, rapid dynamic changes of the wireless environment pose significant challenges to this database-only approach. Dynamic spectrum sensing and its combination with database approaches could address these challenges [10]–[12].

Spectrum sensing is a critical functionality to enable the implementation of dynamic spectrum access in cognitive radio systems [13]. Its goal is to allow secondary users (SUs) to identify the spectrum occupancy states before opportunistically exploiting the temporarily vacant frequency channels, while protecting primary users (PUs) from harmful interferences caused by secondary transmissions. To achieve spectrum awareness over a wide frequency range, wideband spectrum sensing is a highly desirable feature in cognitive radio networks. If a PU reappears over a certain band, the availability of several other possible vacant channels facilitates the seamless handoff from one spectrum channel to another, which reduces secondary data transmission interruptions. However,

Manuscript received May 7, 2016; revised August 13, 2016; accepted August 28, 2016. This work was supported in part by the Engineering and Physical Sciences Research Council (EPSRC) in the U.K. with grant EP/L024241/1, by National Science Foundation of China with grants 61328102/ 61629101, 61571100 and 61631005, by DoD with grant HDTRA1-13-1-0029, and by NSF with grants AST-1547436, ECCS-1508051, CNS-1343155, ECCS-1305979, and CNS-1265227. Part of this paper is presented at the IEEE Global Communications Conference (Globecom), Washington, D.C., USA, December 2016 [1].

Yuan Ma and Yue Gao are with the School of Electronic Engineering and Computer Science, Queen Mary University of London, London E1 4NS, U.K. (emails:{y.ma, yue.gao}@qmul.ac.uk).

Ying-Chang Liang is with the University of Electronic Science and Technology of China, Chengdu 611731, China, and also with the University of Sydney, Australia (e-mail: liangyc@ieee.org).

Shuguang Cui is with the Department of Electrical and Computer Engineering, University of California, Davis, CA, 95616 (email: sgcui@ucdavis.edu).

Digital Object Identifier: 10.1109/JSAC.2016.2605998

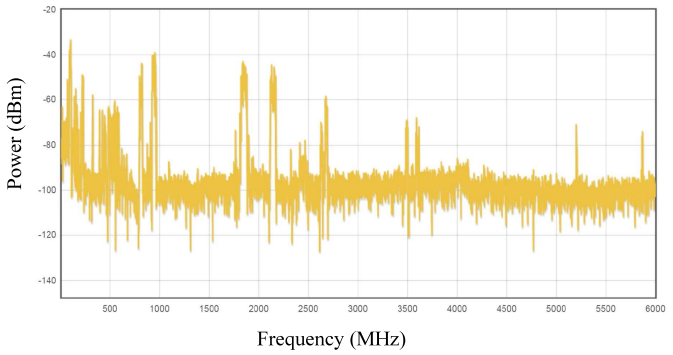

Fig. 1. The real-time spectrum occupancy recorded at QMUL (51.523021°N 0.041592°W) on March 5th, 2016. The figure shows that the spectrum is sparsely occupied on $\mathcal{F} = [0, 6000]$ MHz.

for wideband spectrum sensing, a stringent requirement arises from the Nyquist signal acquisition, which is quite expensive, power-consuming and computation intensive [14]. Due to the energy constraint in compact SUs, efficient real-time wideband spectrum sensing emerges as a crucial challenge for dynamic spectrum sharing in cognitive radio networks.

A simple approach for wideband spectrum sensing is to use a tunable narrowband bandpass filter at the radio-frequency (RF) front-end to scan through all of the narrow channels one by one to detect the existence or non-existence of licensed primary transmissions [15]. However, the sequential nature of such schemes could introduce a long sensing period and thus requires additional energy supply at the SUs. Such delay in the sensing process will also cause missed opportunities or interferences to PUs. In [16], a filter bank algorithm is proposed to process the wideband signal by multiple narrowband bandpass filters with different shifted central frequencies. However, it requires a great number of RF front-end components, e.g., bandpass filters, analog-to-digital converters (ADCs), etc., which may be a serious issue at SUs with restricted energy resources.

Landau in [17] demonstrated that an arbitrary wideband signal can be perfectly reconstructed if being sampled at a rate no less than the total bandwidth of occupied spectrum. As wireless signals over an open spectrum are typically sparse in the frequency domain, it can be recovered by sampling at a rate far less than the Nyquist rate in practice. Compressive sensing were thus introduced to implement wideband spectrum sensing [18]. Although the energy consumption at the wideband signal sampling part is reduced, compressive sensing requires random sub-Nyquist projections [19]. Therefore, custom ADCs with complex hardware that can perform analog mixing or analog matrix multiplication at high frequency are needed in compressive wideband spectrum sensing schemes, which do not work well with low-power commodity hardware [20]–[22]. Moreover, estimating a wideband spectrum from its compressed samples is usually achieved by solving an optimization problem, which requires high computation complexity and thus is hard to implement in compact commodity radios with limited computational capabilities [14].

In [23], a wideband spectrum sensing scheme based on multicoset sampling was proposed, which is a nonuniform sub-Nyquist sampling technique and can be realized using an efficient multi-channel architecture. In addition, a low-speed sub-Nyquist multicoset sampling strategy was proposed in [24] for wideband spectrum sensing without the need of analog front-end processing. However, it requires the knowledge of the spectral support to allow for the perfect reconstruction at the minimal sampling rate provided by the Landau's theorem [17]. To estimate the locations of the occupied channels, Feng and Bresler showed its similarity to the direction of arrival estimation in the traditional sensor array processing, and proposed to use the MUltiple SIgnal Classification (MUSIC) algorithm for signal detection [23], [25]. However, the detection accuracy based on MUSIC algorithm degrades severely when the signal-to-noise ratio (SNR) decreases.

To overcome the SNR degeneration due to multipath fading, shadowing, and noise uncertainty over wireless channels, cooperative spectrum sensing was proposed to improve sensing reliability by exploiting the spatial diversity across multiple SUs [26], where as PUs typically transmit at much higher power levels, a common sparse spectrum support is usually perceived by all the surrounding SUs. To minimize the communication overhead for collaboration, distributed orthogonal matching pursuit (DOMP) was proposed in [27], where each SU estimates the common signal support independently based on its local compressed samples via orthogonal matching pursuit (OMP) and then the estimated supports are fused through a majority voting rule to get the final decision. Although the scheme in [27] is efficient to reduce the transmission overhead, it suffers from the disadvantage of requiring a local detector at each SU and losing certain information due to the non-optimal decision fusion. In [28], Tian proposed a distributed cooperative sensing algorithm based on compressive sensing, in which sampling statistics rather than sensing decisions are exchanged to reach a reliable global fusion. However, it increases the transmission cost and the local l_1 optimization introduces a high computation complexity. In [29], each SU implements wideband channel division to sense K out of L channels and then matrix completion is performed at a fusion center to reconstruct the original spectrum for decision making. As SUs do not sense the whole spectrum, spatial diversity among SUs is not fully exploited and a threshold needs to be predefined to obtain the final decision.

Motivated by the above challenges, this paper first proposes a reliable individual (working at each individual SU node) sub-Nyquist wideband spectrum sensing scheme that can locate active channels blindly, without knowing a *priori* spectral support of the signal before sampling and processing. The only prior information required is an upper bound κ on the possible number of active channels, the maximum bandwidth f_{max}, and the bandwidth of each channel B. Thus there are up to κ out of $L = f_{max}/B$ channels occupied. Following the individual wideband spectrum sensing scheme, an efficient cooperative scheme is then proposed to reduce energy consumption on signal acquisition, processing, and transmission, with certain detection performance guarantee. The major contributions of the proposed scheme are summarized as follows:

- As compact SUs have limited energy and computational capabilities, no signal reconstruction is performed at the SUs to reduce the computation load. Each SU simply implements a multicoset sampler to subsample the wideband signal in the goal of reducing energy consumed on signal sampling. Then a low-dimensional measurement matrix is computed based on subspace decomposition to estimate the active channel locations by recovering the joint signal support of the multiband signal. Compared with the original sub-Nyquist samples, the constructed measurement matrix improves the computation efficiency. As noise distortion is reduced in the constructed measurement matrix, the detection performance is improved in the low SNR regime in comparison with the one solved by the traditional MUSIC algorithm.
- By exploiting the common signal support perceived at all SUs, simultaneous-orthogonal matching pursuit (SOMP) [30] is extended to recover the signal support by jointly fusing measurements shared among the SUs. The index that accounts for the largest residual norm among all SUs is selected in each iteration to achieve accurate detection performance. Different sampling patterns are assigned to different SUs for measurement diversity, with cooperation among SUs reducing the required number of cosets close to the active channel number, where reliable cooperative spectrum sensing is achieved at the minimal sampling rate specified by the Landau's theorem [17].

The rest of the paper is organized as follows. In Section II, signal and network models are described. Section III describes the proposed individual sub-Nyquist wideband spectrum sensing scheme. Section IV develops the centralized cooperative spectrum sensing scheme. Section V analyzes and validates the proposed individual and cooperative schemes, over both simulated and real-world TVWS signals. Conclusions are drawn in Section VI.

II. Signal and Network Models

As shown in Fig. 2, we investigate both the individual ($J = 1$) and cooperative ($J > 1$) wideband spectrum sensing in a cognitive radio network with a fusion center and J SUs, which share the same spectrum with a PU network. To reduce the energy consumption in high frequency signal processing, compressive multicoset sampling is applied to reduce the signal sampling and acquisition costs by exploiting the sparsity in the wireless wideband signal given the low spectrum utilization. With no prior information assumed on the band locations, blind sub-Nyquist sampling and reliable support recovery are implemented at each individual SU to estimate the active channel locations. To further improve the detection performance in low SNR regimes, a centralized cooperative spectrum sensing scheme will be later developed, in which soft fusion is adopted, i.e., SUs send their sampling statistics to the fusion center, where a high-resolution global sensing decision is made. However, traditional soft fusion rules suffer from the disadvantage of large transmission overheads and high computation complexity [31]. Thus, this paper further aims to reduce the transmission and computation overhead by adopting a new fusion rule, without degrading the detection accuracy with cooperative spectrum sensing.

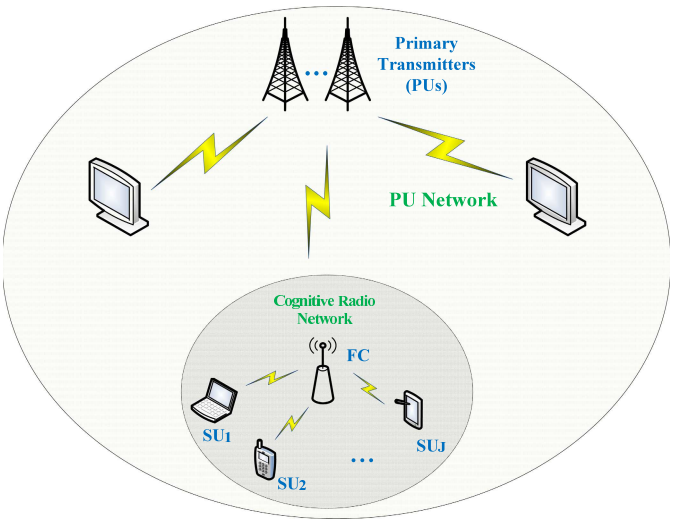

Fig. 2. Cooperative spectrum sensing model in a cognitive radio network.

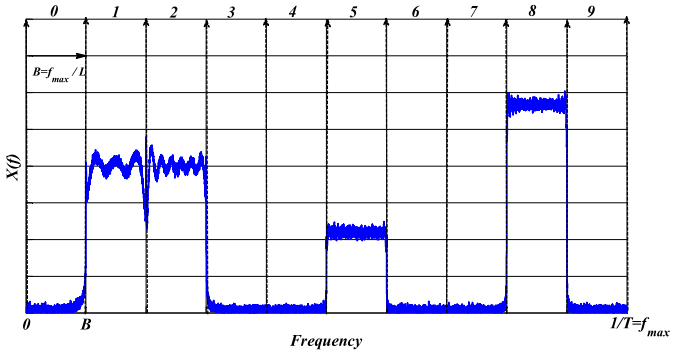

Fig. 3. Signal Spectrum $X(f)$ with $L = 10$ and $\kappa = 4$ active channels, $\boldsymbol{\mathcal{S}} = [1, 2, 5, 8]$.

TABLE I
Notation

$x(t)$	Continuous signal in the time domain
$X(f)$	Fourier Transform of $x(t)$
$\mathbf{A}$	Matrix
$\mathbf{A}_{i,j}$	i-th entry of the matrix $\mathbf{A}$
$\mathbf{A}[i]$	i-th row of the matrix $\mathbf{A}$
$\mathbf{a}_i$	i-th column of the matrix $\mathbf{A}$
$\mathbf{A}^T, \mathbf{A}^H$	The transpose and Hermitian transpose of the matrix $\mathbf{A}$
$\mathbf{A}^\dagger$	Pseudo-inverse of the matrix $\mathbf{A}$
$\mathbf{A}_{\boldsymbol{\mathcal{S}}}$	The matrix made of the columns of $\mathbf{A}$ with indices from $\boldsymbol{\mathcal{S}}$

Without loss of generality, the wideband sparse spectrum to be monitored in the cognitive radio network is $\mathcal{F} = [0,\ f_{max}]$, which is evenly segmented into L narrowbands, each of them with bandwidth B, as illustrated in Fig. 3. The channels are indexed from 0 to $L - 1$. Suppose there are up to κ active channels occupied by PUs during the sensing period with

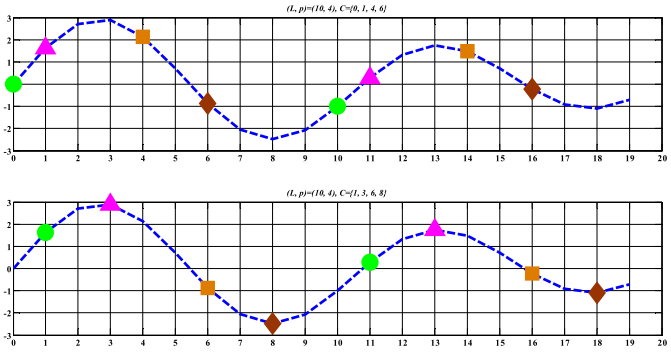

Fig. 4. Examples of two sampling patterns for $(L, p) = (10, 4)$. (a) $C = \{0, 1, 4, 6\}$; (b) $C = \{1, 3, 6, 8\}$.

$\boldsymbol{\mathcal{S}} = [\mathcal{S}_1, \mathcal{S}_2, ..., \mathcal{S}_\kappa]$ denoting the set containing the indices of the occupied channels. Given the prior information on f_{max}, B, and κ, the task of wideband spectrum sensing is to find the presence and locations of the PU signals or equivalently locating the active channel set $\boldsymbol{\mathcal{S}}$. Common notations, as summarized in Table I, are used throughout the paper.

III. Proposed Individual Sub-Nyquist Wideband Spectrum Sensing

In this section, we first consider a non-cooperative blind sub-Nyquist wideband spectrum sensing at each individual SU based on multicoset sampling, i.e., $J = 1$. For convenience, we drop the index j in this section.

A. Blind Sub-Nyquist Wideband Signal Acquisition

Given the prior information on the number of narrowband channels L, multicoset sampling is first executed at each SU by taking non-uniform samples at the time instants $t = (mL + c_i)T$, where $i = 1, ..., p$, $m \in \mathbb{Z}$, and $1/T = f_s$ is the Nyquist sampling rate. The set $\mathcal{C} = \{c_i\}_{i=1}^{p}$, which comprises of p distinct integers chosen from $\{0, 1, ..., L-1\}$, is referred as a (L, p) sampling pattern. Fig. 4 presents two multicoset sampling patterns for $(L, p) = (10, 4)$.

To implement the periodic non-uniform sampling, a multicoset sampler can be realized by p parallel cosets, each of which takes uniform samples at time instants $\{mLT + c_iT\}$, $m \in \mathbb{Z}$, via a decimated sampling rate $\frac{1}{LT} = f_s/L$ with a sampling time offset of $\{c_iT\}$, $i = 1, ..., p$, as shown in Fig. 5.

From the practical standpoint, the non-uniform sub-Nyquist sampling can be realized by a time-interleaved ADC, in which only a subset of channels are used. In [32], [33], efficient fabrications of time-interleaved ADC implemented as a single integrated circuit are proposed. As multicoset sampler only needs fewer channels than the time-interleaved ADC ($p \leq L$), the hardware implementation would be simpler and less power-consuming. In addition, the time offsets can be realized by connecting the antenna to different ADCs using different delay lines.

The measurement sequence of the i-th coset is defined as

$$x_{c_i}[n] = \begin{cases} x(nT), & n = mL + c_i, m \in \mathbb{Z} \\ 0, & \text{otherwise.} \end{cases} \quad (1)$$

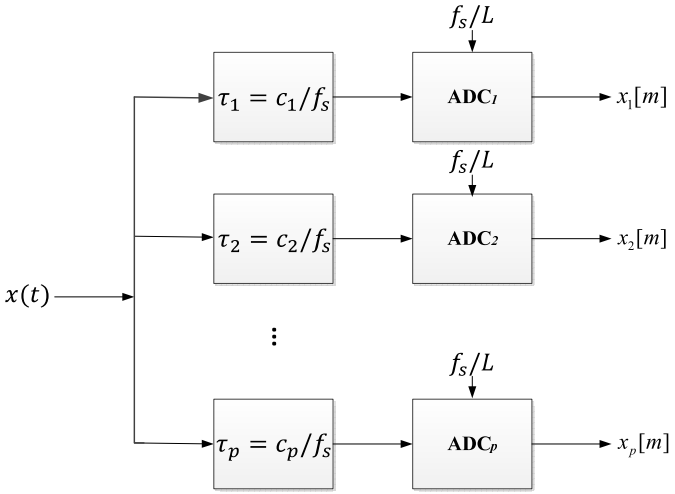

Fig. 5. The parallel implementation of the non-uniform sub-Nyquist sampling.

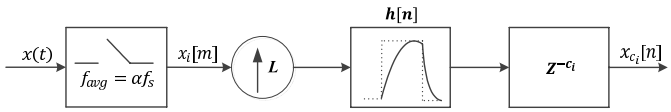

Fig. 6. Flow chart to get the multicoset sampling measurements.

In practice, the ADCs of the parallel cosets provide p sample sequences, given by

$$x_i[m] = x[(mL + c_i)T], \ m \in \mathbb{Z}, \ i = 1, 2, ..., p. \quad (2)$$

In (1), each sequence $x_{c_i}[n]$, $i = 1, ..., p$, contains $L-1$ zeros in between the downsampled signals. To get $x_{c_i}[n]$, each $x_i[m]$ is upsampled by a factor of L:

$$x_{u_i}[n] = \begin{cases} x_i[\frac{n}{L}], & n = mL, \ m \in \mathbb{Z} \\ 0, & \text{otherwise,} \end{cases} \quad (3)$$

and then filtered to get $x_{h_i}[n] = x_{u_i}[n] * h[n]$, where $h[n]$ is an interpolation filter with the frequency response:

$$H(f) = \begin{cases} 1, & f \in [0, B] \\ 0, & \text{otherwise.} \end{cases} \quad (4)$$

The filtered sequence is then delayed with c_i samples to obtain $x_{c_i}[n]$ as

$$x_{c_i}[n] = x_{h_i}[n - c_i]. \quad (5)$$

The whole process to obtain the compressed measurements in multicoset sampling can be implemented as shown in Fig. 6 [23].

The average sampling rate of each (L, p) multicoset sampling pattern is

$$\frac{1}{T_{avg}} = \frac{p}{LT}, \quad (6)$$

where $\alpha = p/L$ is termed as the sub-Nyquist sampling ratio. According to the Landau's theorem [17], α is lower-bounded by the maximum possible spectrum occupancy ratio. However, an average sampling rate above the Landau's rate, which equals the total bandwidth of the occupied spectrum, may not be sufficient for individual blind spectrum recovery, and the

number of cosets $p \geq 2\kappa$ is needed when the band locations are unknown [34].

Applying Fourier transform to $x_{c_i}[n]$ gives the link between its spectrum $X_{c_i}(e^{j2\pi fT})$ and the unknown Fourier Transform of $x(t)$ [23]:

$$\begin{aligned} X_{c_i}(e^{j2\pi fT}) &= \textstyle\sum_{n=-\infty}^{+\infty} x_{c_i}[n]e^{-j2\pi fnT} \\ &= \tfrac{1}{LT}\textstyle\sum_{l=0}^{L-1} \underbrace{X(f+\frac{l}{LT})}_{X_l(f)} e^{j\frac{2\pi}{L}c_i l} \\ &= \tfrac{1}{LT}\textstyle\sum_{l=0}^{L-1} X_l(f) e^{j\frac{2\pi}{L}c_i l} \qquad \forall f \in [0, B], \end{aligned} \tag{7}$$

for every $1 \leq i \leq p$, where $X_l(f)$, $l = 0, ..., L-1$, corresponds to the pieces of the original spectrum $X(f)$ in the channel l, which is shifted to the left by $\frac{l}{LT}$ units such that all L channels are folded into the first narrowband $[0, B]$.

Assume that the observed signal is given by $x(t) = s(t) + n(t)$, where $s(t)$ is the primary signal and $n(t)$ is the additive white Gaussian noise with zero mean and variance σ_n^2. The corresponding Fourier transform is given by $X(f) = S(f) + N(f)$. Define $S_l(f) = S(f + \frac{l}{LT})$, $l = 0, ..., L-1$, and $\mathbf{S}(f) = [S_0(f), S_1(f), ..., S_{L-1}(f)]^T$. Similarly we define $N_l(f)$ and $\mathbf{N}(f)$. We can rewrite (7) into the matrix form as

$$\begin{aligned} &\underbrace{\begin{bmatrix} X_{c_1}(e^{j2\pi fT}) \\ X_{c_2}(e^{j2\pi fT}) \\ \vdots \\ X_{c_p}(e^{j2\pi fT}) \end{bmatrix}}_{\mathbf{Y}(f)} \\ &= \underbrace{\frac{1}{LT}\begin{bmatrix} e^{\frac{j2\pi c_1 0}{L}} & e^{\frac{j2\pi c_1 1}{L}} & \cdots & e^{\frac{j2\pi c_1 (L-1)}{L}} \\ e^{\frac{j2\pi c_2 0}{L}} & e^{\frac{j2\pi c_2 1}{L}} & \cdots & e^{\frac{j2\pi c_2 (L-1)}{L}} \\ \vdots & \vdots & \vdots & \vdots \\ e^{\frac{j2\pi c_p 0}{L}} & e^{\frac{j2\pi c_2 1}{L}} & \cdots & e^{\frac{j2\pi c_p (L-1)}{L}} \end{bmatrix}}_{\mathbf{A}} \\ &\times \underbrace{\begin{bmatrix} X_0(f) \\ X_1(f) \\ \vdots \\ X_{L-1}(f) \end{bmatrix}}_{\mathbf{X}(f)} = \mathbf{A}[\mathbf{S}(f) + \mathbf{N}(f)], \quad \forall f \in [0, B], \end{aligned} \tag{8}$$

where $\mathbf{Y}(f)$ is a matrix whose i-th row is $X_{c_i}(e^{j2\pi fT})$, $\mathbf{X}(f) = [X_0(f), X_1(f), ..., X_{L-1}(f)]^T$ is the unknown spectrum vectors of $x(t)$ in the L channels, and $\mathbf{A} \in \mathbb{C}^{p\times L}$ is a matrix with (i, j)-th element given by

$$\mathbf{A}_{i,j} = \frac{1}{LT} e^{j\frac{2\pi}{L}c_i(j-1)}. \tag{9}$$

As the parameter L in the adopted multicoset sampler is set according to the number of channels in the original spectrum, the support of the original spectrum $supp(\mathbf{S}(f))$ in (8) is equivalent to the active channel index set $\boldsymbol{\mathcal{S}}$. Thus in the proposed wideband spectrum sensing scheme, signal reconstruction is unnecessary and only the support of the spectrum is of interest.

B. Reliable Computation Efficient Joint Sparse Recovery

With multicoset samplers, each SU gets p sample sequences in a matrix from $\mathbf{Y}(f) \in \mathbb{C}^{p\times N}$, where N is the number of samples in each coset. The correlation matrix of the sampled sequence $\mathbf{Y}(f)$ is defined as

$$\mathbf{R} \triangleq \mathbb{E}[\mathbf{Y}(f)\mathbf{Y}^H(f)], \tag{10}$$

where the superscript $()^H$ denotes the Hermitian transpose. Since there is no correlation between the signal and the noise, it follows that

$$\mathbf{R} = \mathbf{A}[\mathbf{R}_s + \sigma_n^2\mathbf{I}]\mathbf{A}^H, \tag{11}$$

where $\mathbf{R}_s \triangleq \mathbb{E}[\mathbf{S}(f)\mathbf{S}^H(f)]$ is the primary signal correlation matrix. Note that $\mathbf{A}$ is a sub-matrix of the complex conjugate of the $L \times L$ discrete Fourier Transform matrix (consisting of p rows indexed by the sampling pattern $\mathcal{C}$) multiplied by a factor of $\frac{1}{LT}$. It is shown that for a larger L, the randomly selected sampling pattern $\mathcal{C}$ enables the matrix $\mathbf{A}$ to have almost orthogonal columns, i.e., $< a_i, a_j >= 0$ for $i \neq j$, and $< a_i, a_j >= \frac{1}{LT^2}$ for $i = j$ with a high probability [19], [35]. Therefore, $\mathbf{R}$ can be derived as:

$$\mathbf{R} = \mathbf{A}\mathbf{R}_s\mathbf{A}^H + \frac{\sigma_n^2}{LT^2}\mathbf{I}, \tag{12}$$

From Parseval's identity [36], the correlation matrix $\hat{\mathbf{R}}$ can be computed directly from the sampled sequence $x_{c_i}[n]$ in the time domain, where $\hat{\mathbf{R}}_{ij} = \frac{1}{N}\sum_{n=1}^{N} x_{c_i}[n]x_{c_j}^H[n]$ [37]. It is shown in [38], [39] that when the number of measurement samples N is much larger than the observation dimension p, $\hat{\mathbf{R}}$ is an accurate estimator of the true correlation matrix.

As there are up to κ active channels occupied during the sensing period, i.e., $\mathbf{R}_s$ has a rank of κ and $\mathbf{A}$ is of full rank, it follows that the rank of $\mathbf{A}\mathbf{R}_s\mathbf{A}^H$ equals κ. Denoting $\lambda_1 \geq \lambda_2 \geq ... \geq \lambda_p$ and $\mu_1, \mu_2, ..., \mu_p$ as the eigenvalues and corresponding eigenvectors of $\mathbf{R}$, respectively, i.e.,

$$\mathbf{R}\mu_i = \lambda_i\mu_i, \ i = 1, ..., p. \tag{13}$$

We then have

$$\begin{aligned} &[\mathbf{A}\mathbf{R}_s\mathbf{A}^H + \tfrac{\sigma_n^2}{LT^2}\mathbf{I}][\mu_1, ..., \mu_p] \\ &\qquad = [\mu_1, ..., \mu_p]\begin{bmatrix} \lambda_1 & & 0 \\ & \lambda_2 & \\ & & \ddots \\ 0 & & \lambda_p, \end{bmatrix}, \end{aligned} \tag{14}$$

i.e.,

$$\begin{aligned} &[\mathbf{A}\mathbf{R}_s\mathbf{A}^H][\mu_1, ..., \mu_p] \\ &= [\mu_1, ..., \mu_p]\begin{bmatrix} \lambda_1 - \frac{\sigma_n^2}{LT^2} & & & 0 \\ & \lambda_2 - \frac{\sigma_n^2}{LT^2} & & \\ & & \ddots & \\ 0 & & & \lambda_p - \frac{\sigma_n^2}{LT^2}, \end{bmatrix}. \end{aligned} \tag{15}$$

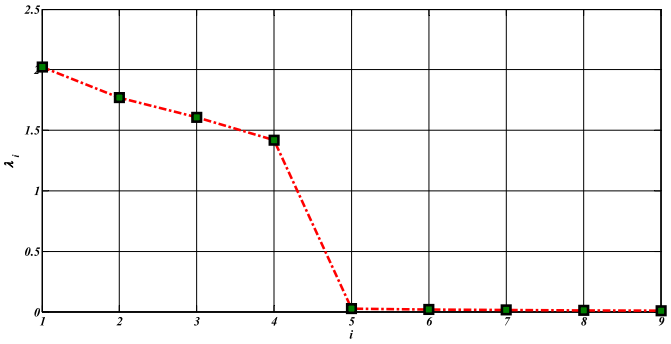

Fig. 7. Eigenvalues of the sample correlation matrix ordered in decreasing order with $p = 9, \kappa = 4$.

Algorithm 1 Joint sparse recovery in SA-SOMP

Require: $\mathbf{R} \in \mathbb{C}^{p\times p}$, $\hat{\kappa}$, $\mathbf{A} = [\mathbf{a}_1, ..., \mathbf{a}_L] \in \mathbb{C}^{p\times L}$
Ensure: $\boldsymbol{\mathcal{S}}$
1: $[\mathbf{U}_s, \boldsymbol{\Lambda}_s] \leftarrow \text{RREVD}(\mathbf{R}, \hat{\kappa})$, $\boldsymbol{\chi}_s = \mathbf{U}_s\sqrt{\boldsymbol{\Lambda}_s}$
2: $t = 0$, $\mathbf{R}_0 = \boldsymbol{\chi}_s$, $\boldsymbol{v}_0 =$, $\boldsymbol{\mathcal{S}} =$
3: **while** $t \leq \hat{\kappa}$ **do**
4: $t \leftarrow t + 1$
5: $l_t = \arg\max_l \parallel \mathbf{a}_l^{\mathbf{H}}\mathbf{R}_{t-1} \parallel_2, l \in 1, ..., L$
6: $\boldsymbol{\mathcal{S}} \leftarrow \boldsymbol{\mathcal{S}} \cup l_t$, $\boldsymbol{v}_t = \mathbf{A}_{\boldsymbol{\mathcal{S}}}^{\dagger}\boldsymbol{\chi}_s$
7: $\mathbf{R}_t \leftarrow \boldsymbol{\chi}_s - \mathbf{A}_{\boldsymbol{\mathcal{S}}}\boldsymbol{v}_t$
8: **end while**
9: **return** $\boldsymbol{\mathcal{S}}$=$\boldsymbol{\mathcal{S}}$-1

Since $\mathbf{A}\mathbf{R}_s\mathbf{A}^H$ has a rank of κ, there must be $p-\kappa$ λ_i's equal to $\frac{\sigma_n^2}{LT^2}$. As $\mathbf{A}\mathbf{R}_s\mathbf{A}^H$ is positive semidefinite, the λ_i's with values equal to $\frac{\sigma_n^2}{LT^2}$ must be the smallest ones of λ_i's. Therefore, we have

$$\lambda_{\kappa+1} = \lambda_{\kappa+2} = ... = \lambda_p = \frac{\sigma_n^2}{LT^2}. \tag{16}$$

As $N \rightarrow \infty$, it follows that except for the κ largest, the eigenvalues of $\mathbf{R}$ are related to the noise variance σ_n^2, as shown in Fig. 7.

Thus $\mathbf{R}$ can be decomposed via the rank-revealing eigenvalue decomposition (RREVD) as

$$\mathbf{R} = \mathbf{U}\boldsymbol{\Lambda}\mathbf{U}^H = \mathbf{U}_s\boldsymbol{\Lambda}_s\mathbf{U}_s^H + \frac{\sigma_n^2}{LT^2}\mathbf{U}_n\mathbf{U}_n^H, \tag{17}$$

where $\mathbf{U} = [\mathbf{U}_s, \mathbf{U}_n]$, $\boldsymbol{\Lambda}_s = \text{diag}\{\lambda_1, ..., \lambda_\kappa\}$ contains the κ non-increasing principal eigenvalues and $\mathbf{U}_s$ contains the corresponding eigenvectors, while $\mathbf{U}_n$ contains the corresponding eigenvectors associated with the smallest $p-\kappa$ eigenvalues $\frac{\sigma_n^2}{LT^2}$. As the noise term only perturbs the eigenvalues, the range of $\mathbf{R}$, spanned by $\mathbf{U}_s$, coincides with the signal subspace spanned by $\mathbf{AS}(f)$, and its orthogonal complement spanned by $\mathbf{U}_n$ is the noise subspace. Therefore, we choose the κ largest eigenvalues $\boldsymbol{\Lambda}_s$ and the corresponding eigenvectors $\mathbf{U}_s$ to construct the measurement matrix as $\boldsymbol{\chi}_s = \mathbf{U}_s\sqrt{\boldsymbol{\Lambda}_s}$; so we can define the following linear system

$$\boldsymbol{\chi}_s = \mathbf{A}\boldsymbol{v}_s, \tag{18}$$

where the support of the sparest solution to (18) converges to the original primary signal, i.e., $supp(\boldsymbol{v}_s) = supp(\mathbf{S}(f))$. Moreover, using $\boldsymbol{\chi}_s \in \mathbb{C}^{p\times\kappa}$ for support recovery instead of $\mathbf{Y}(f) \in \mathbb{C}^{p\times N}$ reduces the transmission overhead and enhances the computational efficiency.

The separation between the signal and noise eigenvalues needs a threshold. Depending on the noise variance and the number of samples, the threshold could vary. To avoid the tricky threshold setting, some information theoretic criteria for the model order selection, such as exponential fitting test (EFT) can be applied for the estimation of the signal support dimension $\hat{\kappa}$ [40].

As only κ active channels assumed to be occupied by primary transmissions, $\boldsymbol{v}_s$ can be approximated to be jointly κ-sparse as it contains no more than κ significant rows. Reconstruction of the unknown matrix $\boldsymbol{v}_s$ with jointly sparse columns in (18) is referred to as the joint sparse problem, which aims to estimate the support of $\boldsymbol{v}_s$ from the measurement matrix $\boldsymbol{\chi}_s$. Some existing greedy algorithms for the sparse recovery problem could be extended to this joint sparse problem, such as SOMP [30]. To improve the detection robustness against noise interference and reduce the computation complexity, SOMP is applied to the constructed low-dimensional measurement matrix $\boldsymbol{\chi}_s$, denoted as subspace-augmented SOMP (SA-SOMP) in this paper. The detailed procedure of the joint sparse recovery in the proposed individual wideband spectrum sensing is summarized in Algorithm 1.

IV. Proposed Cooperative Wideband Spectrum Sensing

As sub-Nyquist measurements are quite vulnerable to channel degradations, cooperation among multiple SUs is necessary in sub-Nyquist wideband sensing. Assume that there are J coexisting SUs within the local region that cooperatively sense the wideband to locate the active channel set $\boldsymbol{\mathcal{S}}$. The received signals at the SUs are from the same primary transmissions but affected differently by fading and shadowing from the common PU transmitter to each SU. Thus all SUs share a common sparse support with different amplitudes.

The proposed cooperative spectrum sensing scheme can be formulated into a three-step framework:

1) Each SU implements a multicoset sampler that independently samples the signal with a different sampling pattern $\mathcal{C}^{(j)}$ from the others, e.g., randomly chosen to allow for more sampling diversity.
2) Measurement matrix $\boldsymbol{\chi}_s^{(j)}$ is constructed at each SU from its sub-Nyquist samples based on subspace decomposition. Then the local matrix $\boldsymbol{\chi}_s^{(j)}$ with the sampling pattern $\mathcal{C}^{(j)}$ is transmitted to the fusion center.
3) The fusion center locates the active channels by jointly fusing measurements shared among the SUs to reach a global sensing decision with enhanced accuracy.

Based on the measurement matrix $\boldsymbol{\chi}_s^{(j)}$ and the sampling pattern $\mathcal{C}^{(j)}$ sent from each SU, the fusion center computes the corresponding reconstruction matrix $\mathbf{A}^{(j)}$ and then locates the active channels by exploiting the common signal support

shared by $\boldsymbol{v}_s^{(j)}$, $j = 1, \cdots, J$, across all SUs. At each SU, the following relationship holds:

$$\boldsymbol{\chi}_s^{(j)} = \mathbf{A}^{(j)} \boldsymbol{v}_s^{(j)}, \ 1 \le j \le J. \tag{19}$$

Exploiting the common sparse support shared by the J SUs, the fusion center fuses measurements sent from all SUs to locate the original active channels. Grouping the rows of $\boldsymbol{v}_s^{(j)}$, $j = 1, ..., J$, with the same indices, forms the matrix $\boldsymbol{\zeta}_s$ as

$$\boldsymbol{\zeta}_s = \Big[\underbrace{\boldsymbol{v}_s^{(1)}[1]^T \cdots \boldsymbol{v}_s^{(J)}[1]^T}_{\boldsymbol{v}_s[1]^T} \cdots \underbrace{\boldsymbol{v}_s^{(1)}[L]^T \cdots \boldsymbol{v}_s^{(J)}[L]^T}_{\boldsymbol{v}_s[L]^T} \Big]^T, \tag{20}$$

where $\boldsymbol{v}_s^{(j)}[i]$ denotes the i-th row of $\boldsymbol{v}_s^{(j)}$ at the j-th SU. Furthermore, $\boldsymbol{\zeta}_s$ can be partitioned as a concatenation of blocks $\boldsymbol{v}_s[l]^T$, $l = 1, ..., L$, and the block size is equal to the number of SUs J. As there are at most κ channels occupied, $\boldsymbol{\zeta}_s$ can be modeled as a block κ-sparse matrix. Thus, in each iteration, the block index that accounts for the largest residual norm among all SUs is selected, i.e.,

$$l_t = \arg\max_{l} \sum_{j=1}^{J} \parallel \mathbf{a}_l^{(j)\mathbf{H}} \mathbf{R}_{t-1}^{(j)} \parallel_2, \ l \in 1, ..., L, \tag{21}$$

where $\mathbf{R}_{t-1}^{(j)}$ is the residue at the $(t-1)$-th iteration at the j-th SU, $\mathbf{a}_l^{(j)}$ is the l-th column in $\mathbf{A}^{(j)}$, and l_t is the selected index. The detailed algorithm for the proposed joint support recovery at the fusion center is described in Algorithm 2, where each SU implements EFT to estimate the signal sparsity $\hat{\kappa}^{(j)}$, and then the fusion center takes the average $\hat{\kappa}$, i.e.,

$$\hat{\kappa} = \frac{1}{J} \sum_{j=1}^{J} \hat{\kappa}^{(j)}, \tag{22}$$

for the number of iterations at the joint support recovery in Algorithm 2.

Based on the measurements shared among the SUs, the detection performance is improved in low SNR regimes. Moreover, thanks to the measurement diversity across multiple SUs given the different sampling patterns, the fusion center could obtain an accurate estimate of the occupied channel locations at the sampling rate approaching the Landau's rate as the number of SUs increases, as shown in Fig. 17. This is due to the fact that the sub-coherence within the block,

$$\mu = \max_{1 \le l \le L} \big(\max_{1 \le i \ne j \le J} ||a_l^{(i)H} a_l^{(j)}|| \big), \tag{23}$$

is substantially smaller than the conventional coherence in the equivalent reconstruction matrix $\mathbf{A}$ [41]. Reconstruction of the block sparse signal in the cooperative sensing scheme therefore can be guaranteed with an eased requirement comparing to the reconstruction in the individual scheme. Therefore, a small number of cosets p proportional to the signal sparsity κ is sufficient for cooperative spectrum sensing. The computation complexity of support recovery at the fusion center could be expressed as $O(\kappa^3 L J)$.

Algorithm 2 Measurement fusion in the proposed centralized cooperative spectrum sensing scheme

Require: $\boldsymbol{\chi}_s^{(j)} \in \mathbb{C}^{p \times \hat{\kappa}^{(j)}}$, $\hat{\kappa}^{(j)}$, $\mathbf{A}^{(j)} = [\mathbf{a}_1^{(j)}, ..., \mathbf{a}_L^{(j)}] \in \mathbb{C}^{p \times L}$
Ensure: $\boldsymbol{\mathcal{S}}$
1: $\hat{\kappa} = \frac{1}{J} \sum_{j=1}^{J} \hat{\kappa}^{(j)}$
2: $t = 0$, $\mathbf{R}_0^{(j)} = \boldsymbol{\chi}_s^{(j)}$, $\boldsymbol{v}_0^{(j)} = \varnothing$, $\boldsymbol{\mathcal{S}} = \varnothing$
3: **while** $t \le \hat{\kappa}$ **do**
4: $t \leftarrow t + 1$
5: $l_t = \arg\max_{l} \sum_{j=1}^{J} \parallel \mathbf{a}_l^{(j)\mathbf{H}} \mathbf{R}_{t-1}^{(j)} \parallel_2, \ l \in 1, ..., L$
6: $\boldsymbol{\mathcal{S}} \leftarrow \boldsymbol{\mathcal{S}} \cup l_t$, $\boldsymbol{v}_t^{(j)} = \mathbf{A}_{\boldsymbol{\mathcal{S}}}^{(j)\dagger} \boldsymbol{\chi}_s^{(j)}$
7: $\mathbf{R}_t^{(j)} \leftarrow \boldsymbol{\chi}_s^{(j)} - \mathbf{A}_{\boldsymbol{\mathcal{S}}}^{(j)} \boldsymbol{v}_t^{(j)}$
8: **end while**
9: **return** $\boldsymbol{\mathcal{S}} = \boldsymbol{\mathcal{S}} - 1$

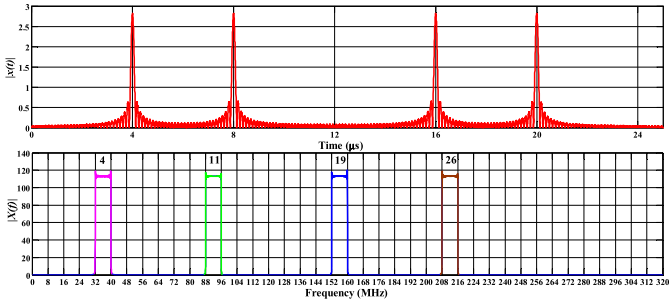

Fig. 8. Simulated signal illustration in time and frequency domains, with $L = 40$, $\kappa = 4$ and $\boldsymbol{\mathcal{S}} = [4, 11, 19, 26]$.

V. Numerical Analysis

This section provides simulation results to evaluate the proposed wideband spectrum sensing scheme using both simulated signals and real-world TVWS signals. We first describe the simulation setup and relevant performance evaluation measures, and then analyze and discuss the obtained results.

A. Experimental Setup and Performance Measures

Consider the received signal $x(t) \in \mathcal{F} = [0, 320]$ MHz containing $L = 40$ channels of equal bandwidth $B = 8$ MHz and up to $\kappa \le L$ active channels. The simulated signal is generated as

$$x(t) = \sum_{i=1}^{\kappa} \sqrt{E_i B} sinc(B(t - t_i)) e^{j2\pi f_i t} + n(t), \tag{24}$$

where $sinc(x) = sin(\pi x)/(\pi x)$, E_i, t_i, and f_i define the energy, time offset, and carrier frequency respectively, on each active channel, and $n(t) \sim \mathcal{N}(0, \sigma_n^2)$ is the additive white Gaussian noise. Thus the spectrum occupancy ratio of primary transmissions can be expressed as $\Omega = \kappa/L$. The signal is observed on a time frame of $T = 25.6$ μs starting at $t = 0$, which corresponds to $T \cdot 320 \cdot 10^6 = 8192$ Nyquist rate samples. Fig. 8 depicts one example of the signal with $\kappa = 4$ active channels, i.e., $\Omega = 10\%$. In this example, $E_i = \{1, 1, 1, 1\}$, $t_i = \{4, 8, 16, 20\}$ μs and the spectrum support is centered at $f_i = \{36, 92, 156, 212\}$ MHz. Thus the active channel set is $\boldsymbol{\mathcal{S}} = [4, 11, 19, 26]$.

(a). Measurement setup at Queen Mary University of London

(b). RFeye sensing node

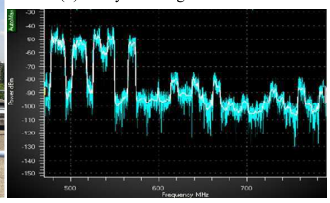

(c). Real-time TVWS signal observed by RFeye sensing node

Fig. 9. Measurements setup for real-time TVWS signals recording at Queen Mary University of London.

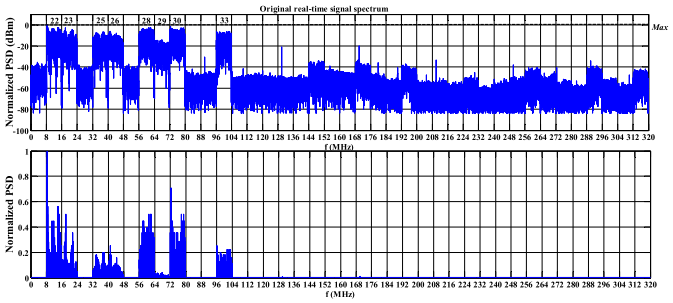

Fig. 10. Normalized power spectrum density (PSD) of the real-time TVWS signal recorded at QMUL, $\boldsymbol{\mathcal{S}} = [22, 23, 25, 26, 28, 29, 30, 33]$

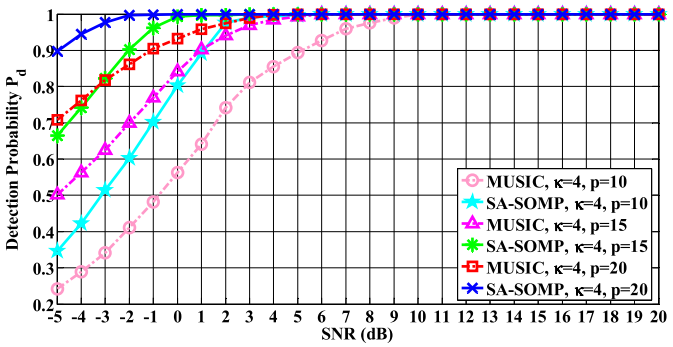

Fig. 11. Detection Probability P_d vs. varying SNR values under different sub-Nyquist sampling ratios $\alpha = p/L$ with $\kappa = 4$.

The real-time TVWS signals are recorded by an RFeye node, an intelligent spectrum monitoring system that can provide real-time 24/7 monitoring of the radio spectrum [5]. The RFeye node is located at (51.523021°N, 0.041592°W), and the height is about 15 meters above the ground, as shown in Fig. 9. There are 40 channels (indexed as Channel 21 - Channel 60) in the recorded TVWS signal, ranging from 470 to 790 MHz and each channel contains either noise only or PU signal with noise. Fig. 10 shows the normalized downconverted TVWS signal in the baseband $\mathcal{F} = [0, 320]$ MHz. Strong DVB-T signal reception at channel set $\boldsymbol{\mathcal{S}} = [22, 23, 25, 26, 28, 29, 30, 33]$ can be observed in the recorded spectrum. Thus the spectrum occupancy ratio is $\Omega = 20\%$.

To quantify the detection performance we compute the detection probability P_d, i.e., the fraction of occupied channels correctly being reported as occupied. The estimated active channel set $\hat{\boldsymbol{\mathcal{S}}}$ is compared against the original signal support $\boldsymbol{\mathcal{S}}$ to compute the detection probability under 2000 trials.

Once the signal support is recovered, reconstruction of the sparse signal has a closed-form solution. Based on the estimated signal support $\hat{\boldsymbol{\mathcal{S}}}$ and the sample sequence $x_{c_i}[n]$, the reconstruction formula can be expressed as

$$x_r[n] = \sum_{q=1}^{\hat{\kappa}} \sum_{i=1}^{p} [\mathbf{A}^{\dagger}_{\hat{\boldsymbol{\mathcal{S}}}+1}]_{i,q} x_{c_i}[n] e^{\frac{j2\pi \hat{\mathcal{S}}_q n}{L}}, \tag{25}$$

where $x_r[n]$ is the reconstruction signal and $\hat{\kappa}$ is the estimated signal sparsity. The accuracy of the reconstructed signal is evaluated by the relative reconstruction mean squared error (MSE) compared with the original signal, which is defined as

$$MSE = \frac{||x_r[n] - x[n]||}{||x[n]||}. \tag{26}$$

B. Individual sub-Nyquist Wideband Spectrum Sensing

To reduce the computation complexity with good noise robustness, subspace decomposition is applied at each SU to derive the measurement matrix $\boldsymbol{\chi}_s$ based on the local sub-Nyquist samples. In this section, the detection performance of the proposed scheme based on SA-SOMP is compared with the one with the MUSIC algorithm, which was proposed in [23] for sparse support recovery with multicoset sampling. The impact of system parameters, such as the SNR, the sub-Nyquist sampling ratio, and the channel occupancy ratio, are also investigated.

1) Spectrum Sensing Performance versus SNR: Fig. 11 shows the detection probability P_d with respect to received SNR ranging from -5 dB to 20 dB. The channel occupancy ratio Ω is assumed to be 10%, such that 4 out of 40 channels are randomly chosen to be occupied. Multicoset samplers with $p = 10, 15, 20$ are used to sample the received signal, corresponding to the sub-Nyquist sampling ratios of $\alpha = p/L = 25\%, 37.5\%, 50\%$. The p integers of each sampling pattern $\mathcal{C}$ are selected randomly out of L. It is shown in Fig. 11 that the performance of the proposed SA-SOMP scheme is superior to that with the MUSIC algorithm, and improves monotonically as SNR increases.

2) Spectrum Sensing Performance versus sub-Nyquist Sampling Ratio: Fig. 12 depicts the reconstructed signal in time and frequency with $p = 15$. Thus the sub-Nyquist sampling ratio is $\alpha = p/L = 37.5\%$. Compared with original signal shown in Fig. 8, the reconstruction MSE is computed to be 2.7%.

To show the relationship between the detection performance and the sub-Nyquist sampling ratio α, we plot P_d against p in Fig. 13. The channel occupancy ratio Ω is still assumed to be 10% ($\kappa = 4$). When the number of cosets p is greater than the number of occupied channels κ only by one, i.e., $\alpha = 12.5\%$, it yields a poor support recovery at individual SUs, thus

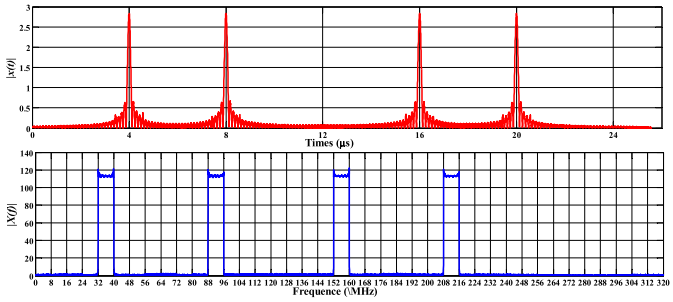

Fig. 12. Reconstructed signal in the time and frequency domains with $p = 15$. The relative reconstruction MSE compared with the original signal in Fig. 8 is 2.7%.

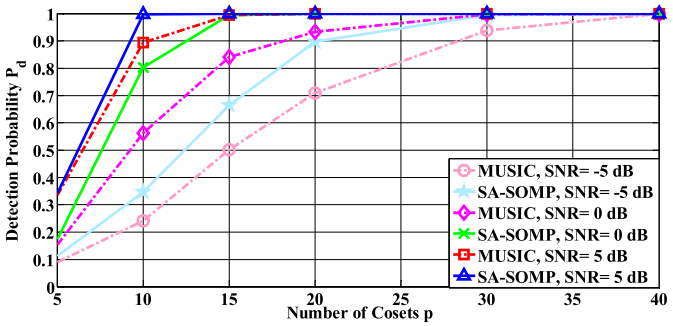

Fig. 13. Detection Probability P_d vs. number of cosets p under different SNR values with $\kappa = 4$, $\alpha = p/L$.

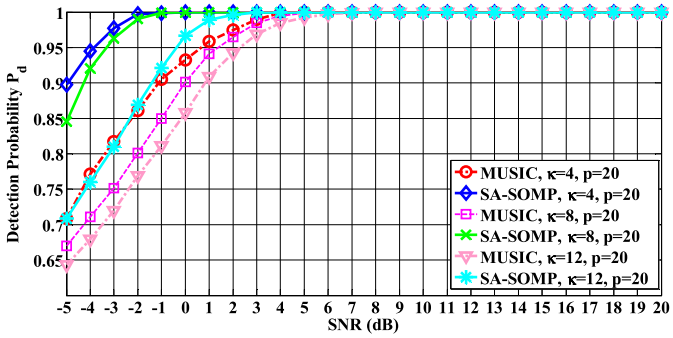

Fig. 14. Detection Probability P_d vs. varying SNR values for different numbers of active channels κ with $p = 20$ ($\alpha = 50\%$).

resulting in a low detection probability. As the number of cosets increases to $p \geq 2\kappa$, better detection performance is achieved, increasing P_d close to 1 under SNR = 5 dB when $p = 10$ for the proposed scheme and outperforming that with the MUSIC algorithm. At SNR = -5 dB, a high detection probability ($P_d \geq 0.9$) is achieved when p increases above 20 ($\alpha = 50\%$) in the proposed scheme, while MUSIC needs more cosets at $p = 30$ ($\alpha = 75\%$).

3) Spectrum Sensing Performance versus Spectrum Occupancy Ratio: Fig. 14 shows the detection performance of the proposed spectrum sensing scheme with different numbers of active channels κ. A multicoset sampler with $p = 20$ is used, such that the sub-Nyquist sampling ratio is $\alpha = 50\%$. The number of active channels κ varies from 4, 8 to 12 and their positions are randomly selected out of $L = 40$ channels.

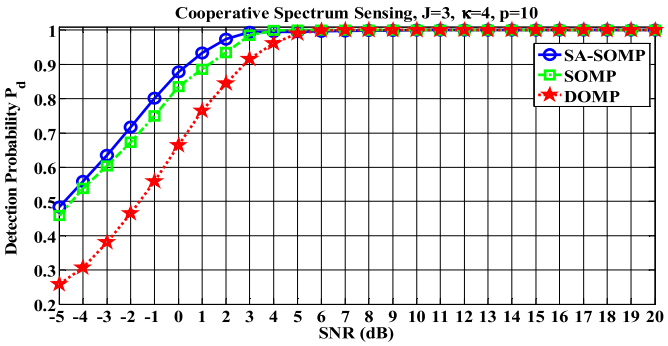

Fig. 15. Global detection probability P_d vs. varying SNR values.

TABLE II
COMPARISON OF COMPLEXITY

Approach	*Transmission Overhead*	*Local Computation Complexity*	*Global Computation Complexity*
SOMP [30]	$O(\kappa N)$	–	$O(\kappa^2 NLJ)$
DOMP [27]	$O(\kappa)$	$O(\kappa^2 NL)$	$O(\kappa JlogJ)$
SA-SOMP	$O(\kappa^2)$	$O(\kappa^2 N + \kappa^3)$	$O(\kappa^3 LJ)$

As Fig. 14 shows, the detection performance degrades as the number of active channels increases, which indicates that more samples should be collected for signal reconstruction to ensure that the detection performance is not degraded as the channel occupancy ratio Ω increases.

C. Cooperative sub-Nyquist Wideband Spectrum Sensing

In this section, the performance of the proposed cooperative wideband spectrum sensing scheme is compared with several other cooperative schemes in terms of transmission and computation complexity and detection accuracy. The impacts of the sub-Nyquist sampling ratio and the number of cooperative SUs on cooperative spectrum sensing are also analyzed.

1) Performance Comparison against SOMP and DOMP: To analyze the efficiency of the proposed scheme in terms of transmission overhead and local/fusion computation complexity, we compare the proposed algorithm with two extreme cases: performing OMP at each SU independently and then fusing the estimated supports via majority rule (termed DOMP), and transmitting the original sub-Nyquist samples and then jointly recovering signal support based on SOMP (termed SOMP), as shown in Table II. Fig. 15 presents the detection performance of the three schemes. Although DOMP has the minimum transmission overhead, its detection performance is the worst. Compared with SOMP, the proposed scheme achieves good detection performance with lower transmission overhead and computation complexity, due to the subspace decomposition.

2) Spectrum Sensing Performance versus Number of SUs and Sub-Nyquist Sampling Ratio: Fig. 16 shows the global detection probability P_d of the proposed cooperative spectrum sensing scheme with different numbers of SUs. It is observed that the detection performance is improved as the number of cooperative SUs increases. This is because as more SUs joints, measurements shared among SUs make the wideband

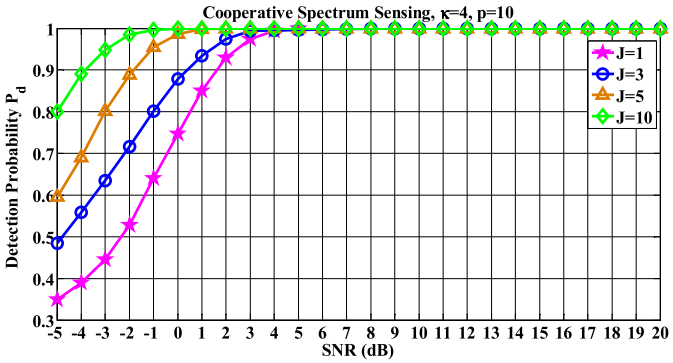

Fig. 16. Global detection probability P_d vs. varying SNR values with different numbers of SUs, $\kappa = 4$ and $p = 10$ ($\alpha = 25\%$).

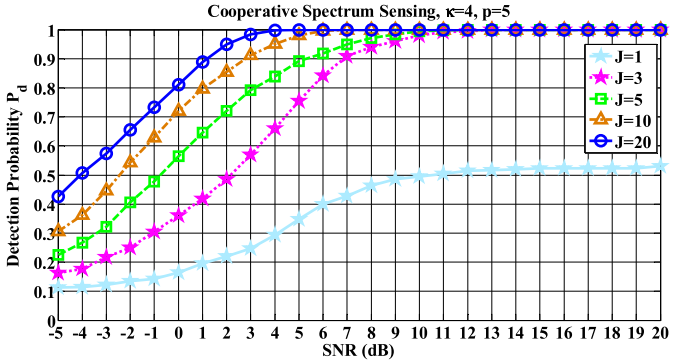

Fig. 17. Global detection probability P_d vs. varying SNR values with different numbers of SUs, $\kappa = 4$ and $p = 5$ ($\alpha = 12.5\%$).

sensing more accurate. By incorporating the observations from multiple SUs, it is possible to achieve the desired detection performance even at low SNR levels. For the desired detection performance, e.g., $P_d \geq 0.9$, individual spectrum sensing ($J = 1$) requires SNR = 2 dB under sub-Nyquist sampling ratio $\alpha = 25\%$ ($p = 10$), while the collaboration of 10 SUs can achieve it at SNR = -4 dB.

For the same wideband signal, Fig. 17 shows the global detection performance when the number of cosets at each SU reduces to $p = 5$. As p is greater than the number of occupied channels κ only by one, individual sensing ($J = 1$) yields poor detection performance even in the high SNR region. Based on measurements fusion among multiple SUs, cooperative spectrum sensing can improve the detection performance as the number of joint SUs J increases. As the value of SNR increases, SU cooperation could achieve highly reliable detection at the minimal sampling rate provided by the Landau's theorem [17], such that a lower number of cosets p is required at each SU.

D. Real-world TVWS Signal Analysis

After the robust performance of the proposed sub-Nyquist wideband spectrum sensing schemes have been validated with simulated signals under individual and cooperative sensing setups, it is further tested over real-world TVWS signals collected by the RFeye sensing node installed in our lab as shown in Fig. 9.

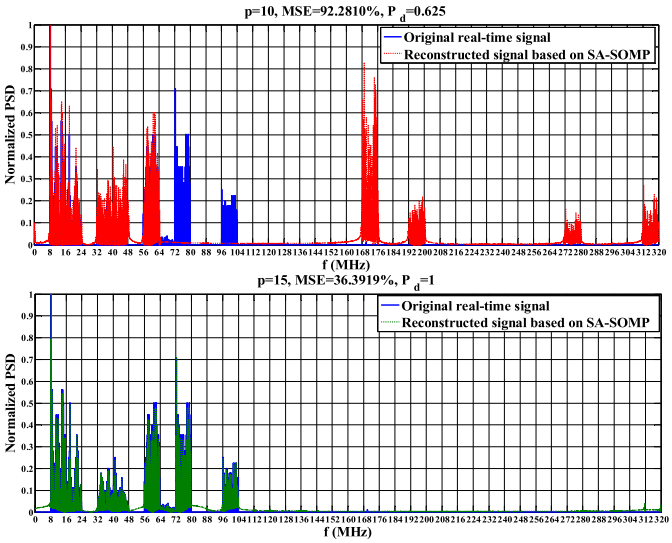

Fig. 18. Normalized PSD of the reconstructed real-world TVWS signal under $p = 10$ and $p = 15$ at individual spectrum sensing.

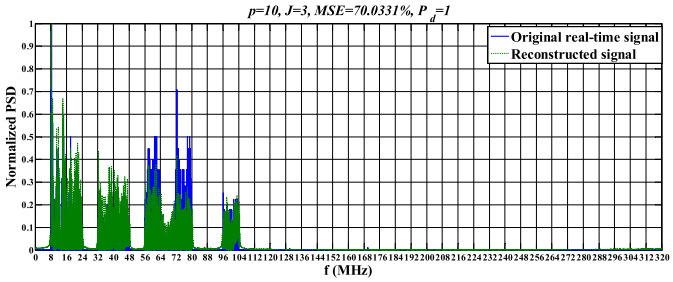

Fig. 19. Normalized PSD of the reconstructed real-world TVWS signal under $p = 10$ at cooperative spectrum sensing of $J = 3$ SUs.

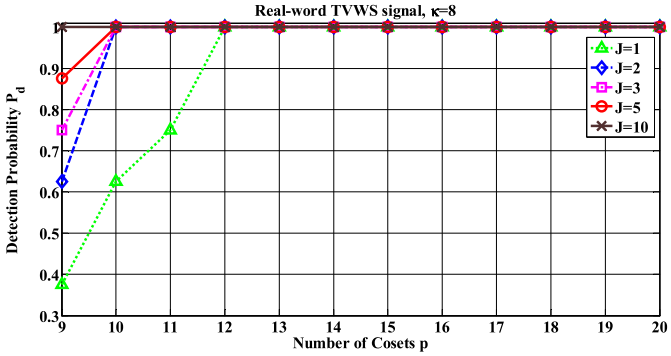

Fig. 20. Detection Probability P_d vs. number of cosets p for the real-world TVWS signal.

To obtain the channel occupancy information over the real-world TVWS signals, a multicoset sampler is firstly applied to subsample the time domain signal, and then the signal support is recovered to estimate the active channel set. Compared with conventional energy detection, which needs to compute the received signal power at each channel and then compare the power against the predefined threshold from the historical statistics to distinguish between the channel occupied by PU signals and a spectrum hole, the proposed wideband spectrum

sensing scheme does not require knowledge of the spectrum information either at the sampling stage or at reconstruction stage; thus the computation and implementation complexity is reduced. In addition, the blind signal support estimation directly obtains the positions of the active channels. Once the signal support is recovered, reconstruction of the wideband signal has a closed-form solution, as presented in (25).

Fig. 18 shows the reconstructed real-world TVWS spectrum at an individual SU equipped with a multicoset sampler, for $p = 10$ and 15, respectively. It is observed that a smaller MSE of the reconstructed signal is achieved under a higher p, but at the cost of a higher sampling rate thus more sample processing. When $p = 10$, i.e., $\kappa < p < 2\kappa$, the individual wideband spectrum sensing scheme misses some occupied channels such that the detection probability P_d reduces to 0.625 and the reconstruction MSE gets higher as well.

We then consider the proposed cooperative spectrum sensing scheme with $p = 10$ and $J = 3$. Due to the measurements sharing among SUs, the fusion center gets an accurate signal support estimation such that the detection probability P_d increases to 1 and the reconstructed signal achieves a good approximation to the original signal, as shown in Fig. 19.

Fig. 20 illustrates the detection probability P_d against the sub-Nyquist sampling ratio α over the real-world TVWS signal. Similarly as shown in Fig. 17, the detection performance is improved as the number of SUs J increases. We see that a smaller number of cosets p proportional to the number of occupied channels κ suffices for the reliable detection in the cooperative cognitive radio networks.

VI. Conclusion

Wideband spectrum sensing is of critical importance to enable dynamic spectrum sharing. In this paper, efficient multicoset sampling based wideband spectrum sensing schemes have been proposed for both individual and cooperative sensing cases to reduce energy consumption on wideband signal acquisition, processing, and transmission, with detection performance guarantee by exploiting the joint sparsity of the multiband signals. Based on a low-rate multi-channel architecture, sub-Nyquist sampling is implemented without complex analog front-end processing. The proposed wideband spectrum sensing schemes locate the active channels blindly without the prior knowledge of the spectral support for the received signal at either the sub-Nyquist sampling or reconstruction stage.

Compared with individual wideband spectrum sensing scheme based on MUSIC, the proposed scheme improves the detection accuracy in low SNR regimes. Exploiting the common signal support perceived at all SUs, the detection accuracy is further improved through cooperative spectrum sensing, in which measurements from multiple SUs are fused jointly to reach a final sensing decision. Based on low-dimensional measurements derived by subspace decomposition, the proposed cooperative spectrum sensing scheme gains better noise robustness while reduces both computation complexity and transmission overhead. Moreover, thanks to the measurement diversity across multiple SUs, reliable sensing results can be achieved at the minimal sampling rate specified by the Landau's theorem, such that the number of cosets p proportional to the signal sparsity κ is shown sufficient for reliable cooperative spectrum sensing.

The robust performance of the proposed wideband spectrum sensing scheme has also been validated over real-world TVWS signals recorded by the RFeye node at QMUL. In comparison with conventional sub-Nyquist wideband spectrum sensing schemes, numerical analysis and experimental results show that the proposed scheme can achieve good detection performance as well as reduced computation and implementation complexity.

References

[1] Y. Ma, Y. Gao, Y.-C. Liang, and S. Cui, "Efficient Blind Cooperative Wideband Spectrum Sensing based on Joint Sparsity," in *Proc. IEEE Global Commun. Conf. (GLOBECOM)*, Washington, D.C., Dec. 2016 (to appear).

[2] P. Kolodzy, "Spectrum policy task force report," *Federal Commun. Commission*, Nov. 2002, ET Docket No. 02-135.

[3] Office of Commun. (Ofcom), "Statement on Cognitive Access to Interleaved Spectrum," Jul. 2009. [Online]. Available: http://stakeholders.ofcom.org.uk/binaries/consultations/cognitive/statement/statement.pdf

[4] G. Ding, J. Wang, Q. Wu, Y.-D. Yao, R. Li, H. Zhang, and Y. Zou, "On the limits of predictability in real-world radio spectrum state dynamics: from entropy theory to 5G spectrum sharing," *IEEE Commun. Mag.*, vol. 53, no. 7, pp. 178–183, Jul. 2015.

[5] RFeye Node. [Online]. Available: http://www.crfs.com/products/rf-sensor-rfeye-node/

[6] O. Holland, S. Ping, Y. Gao, Z. Qin, A. Aijaz, J. Chareau, P. Chawdhry, and H. Kokkinen, "To white space or not to white space: That is the trial within the ofcom TV white spaces pilot," in *Proc. IEEE Int. Conf. on Dynamic Spectrum Access Netw. (DYSPAN)*, Stockholm, Sweden, Sep. 2015, pp. 11–22.

[7] TV White-Spaces. [Online]. Available: http://stakeholders.ofcom.org.uk/spectrum/tv-white-spaces/.

[8] Y. Gao, Z. Qin, Z. Feng, Q. Zhang, O. Holland, and M. Dohler, "Scalable and Reliable IoT Enabled By Dynamic Spectrum Management for M2M in LTE-A," *IEEE Internet of Things Journal*, 2016, (in press).

[9] G. Ding, J. Wang, Q. Wu, Y.-D. Yao, F. Song, and T. A. Tsiftsis, "Cellular-Base-Station-Assisted Device-to-Device Communications in TV White Space," *IEEE J. Sel. Areas Commun.*, vol. 34, no. 1, pp. 107–121, Jan 2016.

[10] N. Wang, Y. Gao, and B. Evans, "Database-augmented spectrum sensing algorithm for cognitive radio," in *Proc. IEEE Int. Conf. on Commun. (ICC)*, London, UK, Jun. 2015, pp. 7468–7473.

[11] Y. Ma, Y. Gao, and C. G. Parini, "Sub-Nyquist rate wideband spectrum sensing over TV white space for M2M communications," in *Proc. IEEE Int. conf. on World of Wireless, Mobile and Multimedia Netw. (WoWMoM)*, Boston, MA, Jun. 2015, pp. 1–6.

[12] Z. Qin, Y. Gao, and C. G. Parini, "Data-assisted low complexity compressive spectrum sensing on real-time signals under sub-nyquist rate," *IEEE Trans. Wireless Commun.*, vol. 15, no. 2, pp. 1174–1185, Feb. 2016.

[13] J. Mitola and G. Maguire JR., "Cognitive Radio: Making software radios more personal," *IEEE Pers. Commun.*, vol. 6, no. 4, pp. 13–18, Aug. 1999.

[14] H. Sun, A. Nallanathan, C.-X. Wang, and Y. Chen, "Wideband spectrum sensing for cognitive radio network: a survey," *IEEE Trans. Wireless Commun.*, vol. 20, no. 2, pp. 74–81, Apr. 2013.

[15] Y. Pei, Y.-C. Liang, K. C. Teh, and K. H. Li, "Energy-Efficient Design of Sequential Channel Sensing in Cognitive Radio Networks: Optimal Sensing Strategy, Power Allocation, and Sensing Order," *IEEE J. Sel. Areas Commun.*, vol. 29, no. 8, pp. 1648–1659, Sep. 2011.

[16] B. Farhang-Boroujeny, "Filter Bank Spectrum Sensing for Cognitive Radios," *IEEE Trans. Signal Process.*, vol. 56, no. 5, pp. 1801–1811, May 2008.

[17] H. J. Landau, "Necessary density conditions for sampling and interpolation of certain entire functions," *Acta Mathematica*, vol. 117, no. 1, pp. 37-52, Jul. 1967.

[18] Z. Tian and G. B. Giannakis, "Compressed sensing for wideband cognitive radios," in *Proc. IEEE Int. conf. on Acoust., Speech and Signal Process. (ICASSP)*, vol. 4, Honolulu, HI, Apr. 2007, pp. 1357–1360.

[19] E. J. Candes, J. Romberg, and T. Tao, "Robust uncertainty principles: Exact signal reconstruction from highly incomplete frequency information," *IEEE Trans. Inf. Theory*, vol. 52, no. 2, pp. 489–509, Feb. 2006.

[20] J. A. Tropp, J. N. Laska, M. F. Duarte, J. K. Romberg, and R. G. Baraniuk, "Beyond Nyquist: Efficient Sampling of Sparse Bandlimited Signals," *IEEE Trans. Inf. Theory*, vol. 56, no. 1, pp. 520–544, Jan. 2010.

[21] M. Mishali and Y. C. Eldar, "From Theory to Practice: Sub-Nyquist Sampling of Sparse Wideband Analog Signals," *IEEE J. Sel. Signal Process.*, vol. 4, no. 2, pp. 375–391, Apr. 2010.

[22] H. Hassanieh, L. Shi, O. Abari, E. Hamed, and D. Katabi, "GHz-wide sensing and decoding using the sparse Fourier transform," in *Proc. IEEE Int. Conf. on Computer Commun. (INFOCOM)*, Toronto, CA, Apr. 2014, pp. 2256–2264.

[23] P. Feng and Y. Bresler, "Spectrum-blind minimum-rate sampling and reconstruction of multiband signals," in *Proc. IEEE Int. conf. on Acoust., Speech and Signal Process. (ICASSP)*, vol. 3, Atlanta, GA, May 1996, pp. 1688–1691.

[24] R. Venkataramani and Y. Bresler, "Optimal sub-Nyquist nonuniform sampling and reconstruction for multiband signals," *IEEE Trans. Signal Process.*, vol. 49, no. 10, pp. 2301–2313, Oct. 2001.

[25] R. Schmidt, "Multiple emitter location and signal parameter estimation," *IEEE Trans. on Antennas and Propagation*, vol. 34, no. 3, pp. 276–280, Mar. 1986.

[26] Z. Quan, S. Cui, A. H. Sayed, and H. V. Poor, "Optimal Multiband Joint Detection for Spectrum Sensing in Cognitive Radio Networks," *IEEE Trans. Signal Process.*, vol. 57, no. 3, pp. 1128–1140, Mar. 2009.

[27] T. Wimalajeewa and P. K. Varshney, "OMP Based Joint Sparsity Pattern Recovery Under Communication Constraints," *IEEE Signal Process. Lett.*, vol. 62, no. 19, pp. 5059–5072, Oct. 2014.

[28] Z. Tian, "Compressed Wideband Sensing in Cooperative Cognitive Radio Networks," in *Proc. IEEE Global Commun. Conf. (GLOBECOM)*, New Orleans, LA8, Nov. 2008, pp. 1–5.

[29] Z. Qin, Y. Gao, M. Plumbley, and C. Parini, "Wideband spectrum sensing on real-time signals at sub-nyquist sampling rates in single and cooperative multiple nodes," *IEEE Trans. Signal Process.*, vol. 64, no. 12, pp. 3106–3117, Jun. 2016.

[30] J. A. Tropp, A. C. Gilbert, and M. J. Strauss, "Simultaneous sparse approximation via greedy pursuit," in *Proc. IEEE Int. conf. on Acoust., Speech and Signal Process. (ICASSP)*, vol. 5, Philadelphia, PA, Mar. 2005, pp. v/721–v/724.

[31] Y.-C. Liang, Y. Zeng, E. C. Peh, and A. T. Hoang, "Sensing-Throughput Tradeoff for Cognitive Radio Networks," *IEEE Trans. Wireless Commun.*, vol. 7, no. 4, pp. 1326–1337, Apr. 2008.

[32] S. M. Louwsma, A. J. M. van Tuijl, M. Vertregt, and B. Nauta, "A 1.35 GS/s, 10 b, 175 mW Time-Interleaved AD Converter in 0.13 μm CMOS," *J. of Solid-State Circuits*, vol. 43, no. 4, pp. 778–786, Apr. 2008.

[33] K. Poulton, R. Neff, B. Setterberg, B. Wuppermann, T. Kopley, R. Jewett, J. Pernillo, C. Tan, and A. Montijo, "A 20 GS/s 8 b ADC with a 1 MB memory in 0.18 μm CMOS," in *Proc. IEEE International Solid-State Circuits Conference, Digest of Technical Papers*, vol. 1, Feb. 2003, pp. 318–496.

[34] M. Mishali and Y. C. Eldar, "Blind Multiband Signal Reconstruction: Compressed Sensing for Analog Signals," *IEEE Trans. Signal Process.*, vol. 57, no. 3, pp. 993–1009, Mar. 2009.

[35] E. J. Candes and T. Tao, "Decoding by linear programming," *IEEE Trans. Inf. Theory*, vol. 51, no. 12, pp. 4203–4215, 2005.

[36] G. B. Arfken, H. J. Weber, and F. E. Harris, *Mathematical Methods for Physicists*, 7th ed. San Diego: Academic Press, 2001.

[37] Y. Zeng and Y.-C. Liang, "Eigenvalue-based spectrum sensing algorithms for cognitive radio," *IEEE Trans. Commun.*, vol. 57, no. 6, pp. 1784–1793, Jun. 2009.

[38] P. Vallet, X. Mestre, and P. Loubaton, "Performance Analysis of an Improved MUSIC DoA Estimator," *IEEE Trans. Signal Process.*, vol. 63, no. 23, pp. 6407 – 6422, Dec. 2015.

[39] B. Nielson and D. R. Cox, *Asymptotic Techniques for Use in Statistics*, 1st ed. London; New York: Chapman and Hall/CRC, 1989.

[40] A. Quinlan, J.-P. Barbot, P. Larzabal, and M. Haardt, "Model order selection for short data: An exponential fitting test (EFT)," *EURASIP J. Adv. Signal Process.*, vol. 2007, Oct. 2006, Art. ID 71953.

[41] Y. C. Eldar, P. Kuppinger, and H. Bolcskei, "Block-Sparse Signals: Uncertainty Relations and Efficient Recovery," *IEEE Trans. Signal Process.*, vol. 58, no. 6, pp. 3042–3054, Jun. 2010.

Yuan Ma (S'15) received double B.Sc. degrees (both with First Class Honors) in telecommunications engineering from Beijing University of Posts and Telecommunications, Beijing, China, and Queen Mary University of London, London, U.K., in 2013. She is currently working towards her Ph.D. degree in the School of Electronic Engineering and Computer Science, Queen Mary University of London since 2013. Her current research interests include cognitive and cooperative wireless networking, sub-Nyquist signal processing, and spectrum analysis, detection and sharing over TV white space.

Yue Gao (S'03-M'07-SM'13) received his Bachelor degree from Beijing University of Posts and Telecommunications in China in 2002, and his MSc and PhD degrees in telecommunications and microwave antennas from Queen Mary University of London (QMUL) in United Kingdom in 2003 and 2007, respectively. Prior to his current role as a Senior Lecturer (Associate Professor), he worked as Research Assistant and Lecturer (Assistant Professor) in the School of Electronic Engineering and Computer Science at QMUL after his PhD degree. He is currently leading the Whitespace Machine Communication (WMC) Lab to develop theoretical research into practice in the interdisciplinary area among antennas, signal processing and spectrum sharing for cyber-physical system (CPS), machine-to-machine (M2M) communications and internet of things (IoT) applications. Dr Gao has authored and co-authored over 100 peer-reviewed journal and conference papers, 2 best paper awards, 1 granted international patent and 2 licensed works to companies, and one book chapter. He is a Senior Member of the IEEE and the principal investigator for TV white space testbed project funded by the Engineering and Physical Sciences Research Council (EPSRC), and a number of projects funded by companies. He has served as the Signal Processing for Communications Symposium Co-Chair for IEEE ICCC 2016, and is serving Publicity Co-Chair for GLOBECOM 2016, Cognitive Radio and Networks Symposia Co-Chair for IEEE GLOBECOM 2017, and the General Co-Chair of the IEEE WoWMoM 2017.

Ying-Chang Liang (F'11) is a Professor in the University of Electronic Science and Technology of China (UESTC), China, and also a Professor in the University of Sydney, Australia. He was a Principal Scientist and Technical Advisor in the Institute for Infocomm Research (I2R), Singapore. His research interest lies in the general area of wireless networking and communications, with current focus on applying artificial intelligence, big data analytics and machine learning techniques to wireless network design and optimization.

Dr Liang was elected a Fellow of the IEEE in December 2010, and was recognized by Thomson Reuters as a Highly Cited Researcher in 2014 and 2015. He received IEEE Jack Neubauer Memorial Award in 2014, the First IEEE Communications Society APB Outstanding Paper Award in 2012, and the EURASIP Journal of Wireless Communications and Networking Best Paper Award in 2010. He also received the Institute of Engineers Singapore (IES)'s Prestigious Engineering Achievement Award in 2007, and the IEEE Standards Association's Outstanding Contribution Appreciation Award in 2011, for his contributions to the development of IEEE 802.22 standard.

Dr Liang is now serving as the Chair of IEEE Communications Society Technical Committee on Cognitive Networks, an Associate Editor of IEEE Transactions on Signal and Information Processing over Network, and an Associate Editor-in-Chief of the World Scientific Journal on Random Matrices: Theory and Applications. He served as Founding Editor-in-Chief of IEEE Journal on Selected Areas in Communications-Cognitive Radio Series, and was the key founder of the new journal IEEE Transactions on Cognitive Communications and Networking. He has been an (Associate) Editor of IEEE Transactions on Wireless Communications, IEEE Transactions on Vehicular Technology, and IEEE Signal Processing Magazine. Dr Liang was a Distinguished Lecturer of the IEEE Communications Society and the IEEE Vehicular Technology Society, and has been a member of the Board of Governors of the IEEE Asia-Pacific Wireless Communications Symposium since 2009. He served as Technical Program Committee (TPC) Chair of CROWN'08 and DySPAN'10, Symposium Chair of ICC'12 and Globecom'12, General Co-Chair of ICCS'10 and ICCS'14. He serves as TPC Chair and Executive Co-Chair of Globecom'17 to be held in Singapore.

Shuguang Cui (S'99-M'05-SM'12-F'14) received his Ph.D in Electrical Engineering from Stanford University, California, USA, in 2005. Afterwards, he has been working as assistant, associate, and full professor in Electrical and Computer Engineering at the Univ. of Arizona and Texas A&M University. He is currently a full professor in Electrical and Computer Engineering at the Univ. of California-Davis. His current research interests focus on data oriented large-scale information analysis and system design, including large-scale distributed estimation and detection, information theoretical approaches for large data set analysis, complex cyber-physical system design, and cognitive network optimization. He was selected as the Thomson Reuters Highly Cited Researcher and listed in the Worlds' Most Influential Scientific Minds by ScienceWatch in 2014. He was the recipient of the IEEE Signal Processing Society 2012 Best Paper Award. He has served as the general co-chair and TPC co-chairs for many IEEE conferences. He has also been serving as the area editor for IEEE Signal Processing Magazine, and associate editors for IEEE Transactions on Big Data, IEEE Transactions on Signal Processing, IEEE JSAC Series on Green Communications and Networking, and IEEE Transactions on Wireless Communications. He was the elected member for IEEE Signal Processing Society SPCOM Technical Committee (2009-2014) and the elected Vice Chair for IEEE ComSoc Wireless Technical Committee (2015-2016). He is a member of the Steering Committee for both IEEE Transactions on Big Data and IEEE Transactions on Cognitive Communications and Networking. He is also a member of the IEEE ComSoc Emerging Technology Committee. He was elected as an IEEE Fellow in 2013 and an IEEE ComSoc Distinguished Lecturer in 2014.